Restoring GABAergic inhibition rescues memory deficits in a Huntington's disease mouse model

Zahra Dargaei[a], Jee Yoon Bang[b], Vivek Mahadevan[a,1], C. Sahara Khademullah[a], Simon Bedard[a], Gustavo Morrone Parfitt[a,b], Jun Chul Kim[b], and Melanie A. Woodin[a,2]

[a]Department of Cell and Systems Biology, University of Toronto, Toronto, ON M5S 3G5, Canada; and [b]Department of Psychology, University of Toronto, Toronto, ON M5S 3G3, Canada

Edited by Mu-ming Poo, Chinese Academy of Sciences, Shanghai, China, and approved January 5, 2018 (received for review September 25, 2017)

Huntington's disease (HD) is classically characterized as a movement disorder, however cognitive impairments precede the motor symptoms by ∼15 y. Based on proteomic and bioinformatic data linking the Huntingtin protein (Htt) and KCC2, which is required for hyperpolarizing GABAergic inhibition, and the important role of inhibition in learning and memory, we hypothesized that aberrant KCC2 function contributes to the hippocampal-associated learning and memory deficits in HD. We discovered that Htt and KCC2 interact in the hippocampi of wild-type and R6/2-HD mice, with a decrease in KCC2 expression in the hippocampus of R6/2 and YAC128 mice. The reduced expression of the Cl^--extruding cotransporter KCC2 is accompanied by an increase in the Cl^--importing cotransporter NKCC1, which together result in excitatory GABA in the hippocampi of HD mice. NKCC1 inhibition by the FDA-approved NKCC1 inhibitor bumetanide abolished the excitatory action of GABA and rescued the performance of R6/2 mice on hippocampal-associated behavioral tests.

Huntington's disease | synaptic inhibition | GABA | chloride | learning

Huntington's disease (HD) is primarily characterized by progressive motor incoordination and involuntary movements that result from neurodegeneration of the striatum (1). However, cognitive and behavioral impairments involving the cortex and hippocampus emerge in the early stages of the disease and precede the motor impairments by more than a decade. HD patients display hippocampal-dependent learning and memory deficits (2–4), and mouse models of HD have alterations in excitatory synaptic plasticity in the hippocampus and impaired spatial cognition (5–10). However, the learning and memory functions of the hippocampus do not rely solely on synaptic plasticity of glutamatergic synapses. It has recently become clear that inhibitory GABA-releasing interneurons are required for hippocampal-dependent learning and memory tasks (11). For example, inactivating somatostatin-positive interneurons in the hippocampus prevents contextual fear conditioning (12), while ablation of parvalbumin-positive CA1 interneurons impairs spatial working memory (13). The tight link between inhibition and learning and memory is also clear in neurodegenerative disease, where reduced inhibition underlies neuronal network dysfunction in an Alzheimer's disease mouse model (14) and restoring inhibition rescues the associated memory deficits (15, 16). Despite the requirement of inhibition for learning and memory and the deficits in hippocampal-dependent learning and memory in HD, inhibitory synaptic transmission in the hippocampus has not been characterized in the HD brain.

Synaptic inhibition in the brain is largely mediated by GABA acting on Cl^--permeable $GABA_A$ receptors (17). The polarity of $GABA_A$ receptor signaling depends on the precise regulation of two cation-chloride cotransporters, KCC2 ($K^+ \cdot Cl^-$) and NKCC1 ($Na^+ \cdot K^+ \cdot 2Cl^-$) (18, 19). NKCC1-mediated Cl^- accumulation into neurons leads to excitatory GABA early in development, whereas KCC2-mediated Cl^- extrusion leads to inhibitory GABA in mature neurons (18, 19). When KCC2 and/or NKCC1 expression is disrupted, the neuronal Cl^- gradient can collapse, resulting in a profound disruption of inhibition, which contributes to numerous neurological disorders including epileptic seizures (20), Down syndrome (21), and autism spectrum disorder (ASD) (22). Restoring the neuronal Cl^- gradient can rescue GABAergic inhibition deficits and behavioral phenotypes in animal models in several neurological disorders including ASD (22) and Down syndrome (21). Furthermore, KCC2-mediated Cl^- regulation directly controls synapse specificity of long-term potentiation at CA1 synapses in the hippocampus of mature animals (23).

A prominent group of Htt interactors are proteins involved in synaptic transmission, and their altered interaction with mutant Htt (mHtt) is suggested to contribute to abnormal synaptic transmission in HD (24). Recent proteomic studies revealed that the KCC2 encoding gene, *Slc12A5*, is highly enriched in Htt proteome (25, 26), but despite the strong correlation, this interaction has not been validated. Furthermore, a bioinformatic analysis of the unfolded protein response (UPR)-regulated genes in HD reveals an increase in NKCC1 mRNA and a decrease in KCC2 mRNA (27), which is significant because UPR is implicated in numerous neurodegenerative diseases including HD (28–30). Based on the previous data linking (m)Htt and Cl^- transporters (25, 26) and the important role of inhibition in learning and memory, we hypothesized that KCC2 function is dysregulated in the HD brain, resulting in weakened inhibitory GABAergic transmission, which contributes to the hippocampal-dependent learning and memory deficits that emerge early in HD.

Significance

Huntington's disease (HD) is a fatal neurodegenerative disorder that currently has no cure. Although HD is classically considered a motor disorder, HD patients experience learning and memory deficits years before the onset of motor symptoms, and these deficits resemble those observed in HD mouse models. In this work, using transgenic mouse models of HD, we demonstrate that the action of the neurotransmitter GABA has switched from inhibitory to excitatory. By treating HD mice with a clinically used diuretic (bumetanide), which restores inhibitory GABA, we rescued the learning and memory deficits. Our data suggest a potential therapeutic approach for the treatment of the cognitive deficits in early HD that can improve patient quality of life and reduce caregiver burden.

Author contributions: Z.D., J.C.K., and M.A.W. designed research; Z.D., J.Y.B., V.M., C.S.K., S.B., and G.M.P. performed research; Z.D., J.Y.B., V.M., and C.S.K. analyzed data; and Z.D. and M.A.W. wrote the paper.

The authors declare no conflict of interest.

This article is a PNAS Direct Submission.

[1]Present address: Section on Cellular and Synaptic Physiology, National Institute of Child Health and Human Development, Bethesda, MD 20892.

[2]To whom correspondence should be addressed. Email: m.woodin@utoronto.ca.

This article contains supporting information online at www.pnas.org/lookup/suppl/doi:10.1073/pnas.1716871115/-/DCSupplemental.

We determined that Htt and KCC2 interact in the hippocampus of both wild-type (WT) and the R6/2 transgenic mouse model of HD. We also discovered that decreased KCC2 and increased NKCC1 expression in the hippocampi HD mice result in a depolarizing shift in the reversal potential for $GABA_A$ receptor-mediated Cl^- currents (E_{GABA}), which renders $GABA_A$ receptor signaling excitatory in R6/2 mice. The treatment of R6/2 mice with the FDA-approved NKCC1 inhibitor bumetanide restored E_{GABA} to the value seen in WT mice, abolished the excitatory action of GABA, and rescued the hippocampal-associated memory deficits in R6/2 mice.

Results

Htt Interacts with KCC2 in the Hippocampus of WT and R6/2 Mice. Based on the bioinformatic and proteomic studies linking KCC2 and Htt (25, 26), we first determined biochemically whether KCC2 and Htt interact. We performed coimmunoprecipitation (co-IP) assays from hippocampal brain lysates prepared from WT and the R6/2 mouse model of HD. R6/2 mice express the exon 1 human Htt with 120 CAG repeats (31) and develop a relatively fast progressing neurological phenotype similar to HD. At birth, R6/2 mice are indistinguishable from their littermate controls and develop normally until ∼8 wk of age (31). Because we hypothesized that KCC2 dysfunction and weakened synaptic inhibition contribute to the learning and memory deficits in early stages of the disease, we performed the co-IP on hippocampal brain lysates collected from 7-wk-old WT and R6/2 mice. Using anti-Htt antibodies, we found that Htt precipitates KCC2, indicating the existence of a KCC2–Htt complex in vivo (Fig. 1*A* and *SI Appendix*, Fig. S1 *A–D*). KCC2 exists as both monomers (∼140 kDa) and oligomers (>250 kDa), with the oligomeric form believed to be the functional form of the transporter in the mature brain (32, 33). We found that Htt interacts with both monomeric and oligomeric KCC2. As a control, we probed for NKCC1, which is not present in the Htt interactome (26), and found no interaction with Htt (Fig. 1*A* and *SI Appendix*, Fig. S1*E*). To determine whether KCC2 can interact with mHtt, we performed co-IP assays in COS-7 cells transfected with KCC2 and the normal or expanded polyglutamine tract of Htt (Htt-FL-15Q-HA and Htt-FL-128Q-HA, respectively). We found that both normal and mutant forms of Htt could precipitate KCC2 (Fig. 1*B* and *SI Appendix*, Fig. S2).

KCC2 and NKCC1 Protein Expression Are Altered in the Hippocampus of HD Mice. mHtt interacts with proteins involved in synaptic transmission and can alter the function, cellular distribution, and total expression of these interacting proteins (34–36). To determine if the KCC2–mHtt interaction alters KCC2 protein expression, we performed Western blot analysis from hippocampal brain lysates and found a significant decrease in total KCC2 protein (oligomer + monomer) at 7 wk in R6/2 mice relative to WT (Fig. 2*A* and *SI Appendix*, Fig. S3 *A–C*; WT, 0.59 ± 0.08; R6/2, 0.33 ± 0.04; $P = 0.0104$). We also observed a significant decrease in fluorescence intensity of KCC2 at the surface membrane in the hippocampus of R6/2 mice compared with WT controls (Fig. 2*E* and *SI Appendix*, Fig. S4; WT, 69.07 ± 2.09; R6/2, 46.27 ± 2.03; $P < 0.0001$). To determine if the altered KCC2 and NKCC1 expression in the R6/2 hippocampus is common in HD, we repeated our protein expression experiments in the YAC128 mouse model of HD, which expresses full-length human Htt with 128 CAG repeats (37). This model has a later onset of motor symptoms (compared with R6/2) and closely recapitulates the motor dysfunction and neuropathology observed in human HD (37). We performed Western blots on hippocampal brain lysates collected from 9-wk-old WT and YAC128 mice. Consistent with our findings in R6/2, we also observed a significant decrease in KCC2 expression in YAC128 mice (0.80 ± 0.07) compared with WT (1.16 ± 0.12; $P = 0.030$) (Fig. 2*B* and *SI Appendix*, Fig. S3 *G* and *H*). We also probed for NKCC1, because in other neurological disorders where KCC2 is decreased, increases in NKCC1 have been reported (38, 39) and are thought to represent a reversion to an immature GABAergic phenotype (39, 40). Interestingly, although NKCC1 is not in the Htt interactome (25, 26) and does not co-IP with Htt (Fig. 1*A*), we found a significant increase in NKCC1 protein expression at 7 wk in R6/2 mice (Fig. 2*C* and *SI Appendix*, Fig. S3 *D–F*; WT, 0.53 ± 0.09; R6/2, 2.02 ± 0.37; $P = 0.0104$) but not YAC128 mice (Fig. 2*D* and *SI Appendix*, Fig. S5 *I* and *J*; WT, 1.30 ± 0.14; YAC128, 1.53 ± 0.21; $P = 0.368$).

To determine if gene transcription underlies the alterations in protein expression, we performed real-time qPCR on samples from R6/2 and WT mice using isoform-specific amplification of *Slc12A5* (KCC2) and *Slc12A2* (NKCC1). We used previously identified stable control genes for R6/2 mice (*Rpl13a*, *ATP5b*, *Ubc*, *Canx*) (41) and found a significant decrease in KCC2 mRNA from R6/2 mice (7 wk old) compared with WT, consistent with bioinformatic predictions (27) (Fig. 2*F* and *SI Appendix*, Fig. S5

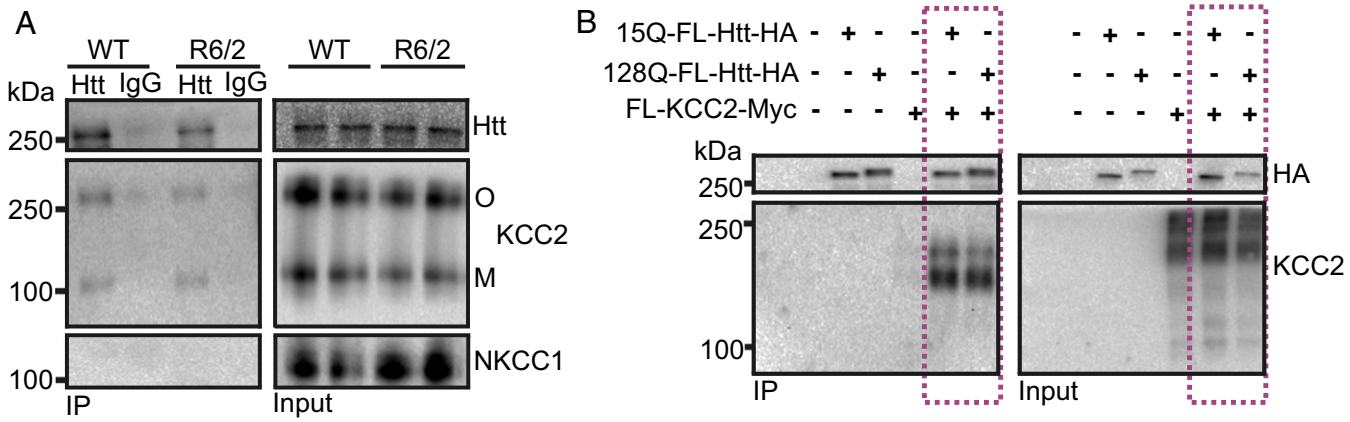

Fig. 1. KCC2 and Htt interact in the hippocampus of WT and R6/2 mice. (*A*) Native Htt complexes from C12E9-solubilized hippocampal brain lysates immunoprecipitated with anti-Htt antibodies and immunoblotted with the antibodies indicated at right (Htt, KCC2, NKCC1). Shown is a representative example of five independent biological replicates (full blots presented in *SI Appendix*, Fig. S1). Input, input fraction (2% of IP); IP, immunoprecipitation; M, monomer; O, oligomer. (*B*) Co-IP experiments performed in COS-7 cells transfected with 15Q-Htt-HA, or 128Q-Htt-HA and KCC2-Myc solubilized in RIPA buffer, immunoprecipitated with anti-HA antibodies, and immunoblotted with the antibodies indicated at right (KCC2, HA). Shown is a representative example of five independent biological replicates (full blots presented in *SI Appendix*, Fig. S2).

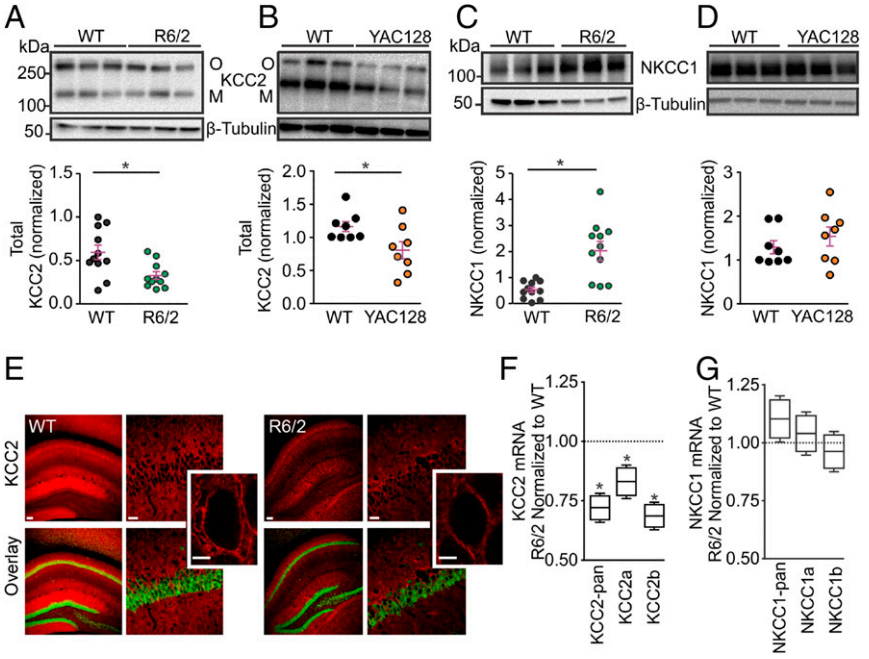

Fig. 2. KCC2 and NKCC1 protein expression is altered in the hippocampi of HD mice. (*A*, *Top*) Representative immunoblot images for KCC2 in protein extracts from samples of hippocampus lysate from WT and R6/2. (*A*, *Bottom*) Quantification of total KCC2 (oligomer + monomer) in WT ($n = 11$) and R6/2 ($n = 11$) normalized to β-Tubulin ($P = 0.0104$; Student's unpaired t test). (*B*) Similar to *A* but for WT ($n = 8$) and YAC128 ($n = 8$) ($P = 0.030$; Student's unpaired t test). (*C*, *Top*) Representative immunoblot images for NKCC1 in protein extracts from samples of hippocampus lysates from WT and R6/2. (*C*, *Bottom*) Quantification of NKCC1 in WT ($n = 11$) and R6/2 ($n = 11$) normalized to β-Tubulin ($P = 0.0104$; Mann–Whitney test). (*D*) Similar to *C* but for WT ($n = 8$) and YAC128 ($n = 8$) ($P = 0.368$; Student's unpaired t test). (Full blots are presented in *SI Appendix*, Fig. S3.) For all panels, circles indicate values from individual animals. (*E*) Representative confocal images of hippocampal sections from 7-wk-old WT (*Left*) and R6/2 (*Right*) mice double labeled for KCC2 (*red*) and NeuN (*green*). [Scale bars, 100 μm (*Left*), 25 μm (*Right*), and 5 μm (*Insets*).] See *SI Appendix*, Fig. S4 for quantifications. (*F*) Relative fold difference of pan-KCC2 ($P = 0.011$), KCC2a ($P = 0.033$), KCC2b ($P = 0.046$), and (*G*) pan-NKCC1 ($P = 0.547$), NKCC1a ($P = 0.822$), NKCC1b ($P = 0.852$) abundance in R6/2 ($n = 5$) hippocampi normalized to WT ($n = 5$) using Student's unpaired t test. See *SI Appendix*, Fig. S5 for NKCC1 or KCC2 mRNA quantifications normalized to the geometric means of housekeeping genes. All summary figures represent mean ± SEM. *$P < 0.05$.

A–C). The same set of control genes, however, showed variability between WT and YAC128 hippocampus and showed no statistical differences in the relative expression of KCC2 mRNA expression (*SI Appendix*, Fig. S5*D*). Pan-NKCC1 transcript, but not NKCC1a/b, was also significantly increased in R6/2 hippocampal samples but only compared with one of the control genes, *Rpl13a* (Fig. 2*G* and *SI Appendix*, Fig. S5 *A–C*).

E_{GABA} Is Depolarized in CA1 Neurons from HD Hippocampi. In mature neurons, relatively high expression of KCC2 results in low levels of intracellular Cl^- and a hyperpolarized reversal potential for GABA (E_{GABA}) (18, 19). When KCC2 is reduced and/or NKCC1 is increased, E_{GABA} depolarizes and can even render GABA excitatory (21, 42, 43). To address whether the altered protein levels of KCC2 and NKCC1 in the hippocampus of R6/2 mice disrupt the polarity of GABA (hyperpolarizing vs. depolarizing), we recorded E_{GABA} from CA1 pyramidal neurons in hippocampal slices using whole-cell patch-clamp recordings. We found that E_{GABA} from R6/2 mice was significantly depolarized (−58.05 ± 1.68 mV) compared with WT mice (−67.45 ± 1.47 mV; $P = 0.0009$; Fig. 3 *A* and *B*), with no significant differences in the resting membrane potential (WT, −65.88 ± 2.12 mV; R6/2, −67.82 ± 1.23 mV; $P = 0.41$; Fig. 3*D*) or synaptic conductance (WT, 5.20 ± 0.98 pS; R6/2, 5.23 ± 0.75 pS; $P = 0.97$; Fig. 3*E*). During whole-cell patch-clamp recordings, the contents of the intracellular pipette dialyze with cytoplasm, which can alter the Cl^- gradient and E_{GABA}. To preserve the intracellular Cl^- concentration, we performed gramicidin-perforated patch-clamp recordings and again found that the E_{GABA} was significantly depolarized in R6/2 hippocampal neurons compared with WT mice (WT, −71.37 ± 1.70 mV; R6/2, −62.07 ± 3.095 mV; $P = 0.02$; Fig. 3*C*). KCC2 function is optimally tested in the presence of a Cl^- load, which simulates the physiological context during inhibition (44). To examine KCC2 function in the presence of a Cl^- load to drive transporter function, we loaded the intracellular compartment with Cl^- through the whole-cell patch pipette (44) (30 mM Cl^-). Again, we found a significant depolarizing shift in E_{GABA} in R6/2 hippocampal neurons compared with WT (WT, −50.73 ± 3.59 mV; R6/2, −39.13 ± 2.32 mV; $P = 0.01$; Fig. 3*C*). To determine if E_{GABA} was also depolarized in YAC128 hippocampal neurons (9 wk old), we repeated our whole-cell patch-clamp recordings and again found a significant depolarization of E_{GABA} compared with age-matched controls (WT, −70.93 ± 1.61 mV; YAC128, −62.18 ± 1.72 mV; $P = 0.004$; Fig. 3 *F* and *G*) with no significant change in resting membrane potential (WT, −66.71 ± 2.25 mV; YAC128, −66.62 ± 1.79; $P = 0.97$; Fig. 3*H*).

Lastly, we investigated whether altered KCC2 and NKCC1 expression and depolarized E_{GABA} also occur in other brain regions. We performed Western blot analysis and whole-cell patch-clamp recording in the cortex of R6/2 and WT mice. We found an increase in the expression of NKCC1 and a decrease in the expression of KCC2 in the cortices of R6/2 mice relative to that in WT mice (*SI Appendix*, Fig. S6). E_{GABA} was also depolarized in the somatosensory area L4/5 of the cortex in R6/2 mice compared with WT (*SI Appendix*, Fig. S7).

GABAergic Inhibition Is Converted into Excitation in R6/2 Mice. A depolarization of E_{GABA} can result in loss of inhibitory drive and increase neuronal excitability. To directly test this, we made cell-attached patch-clamp recordings from CA1 pyramidal neurons and recorded the baseline spontaneous spiking activity in WT and

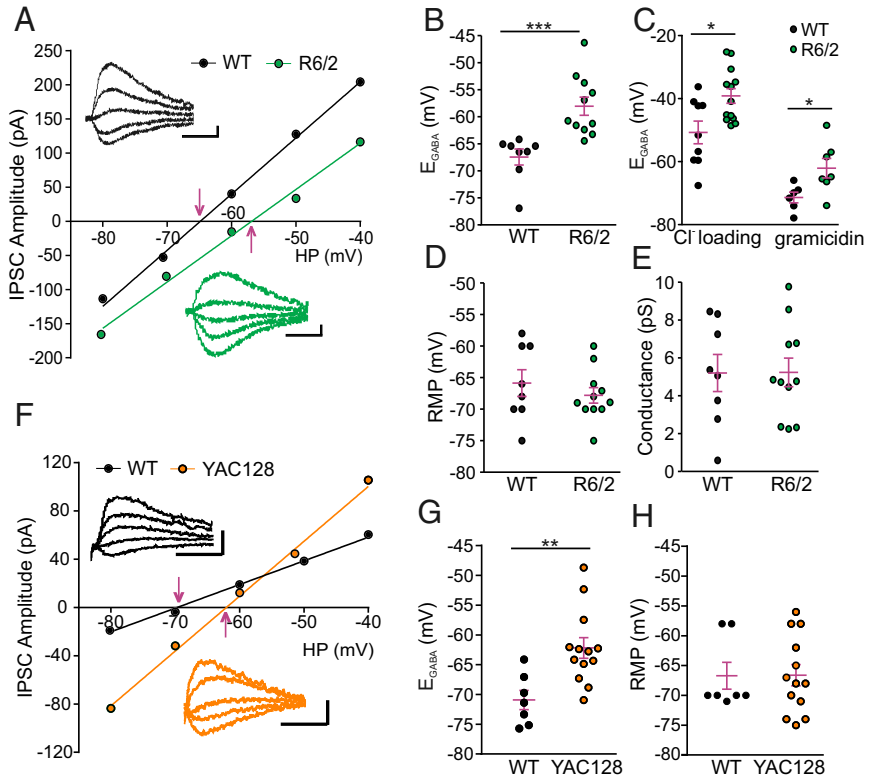

Fig. 3. E_{GABA} is depolarized in hippocampal CA1 pyramidal neurons of HD mice. (*A* and *F*) Example current–voltage curves of inhibitory postsynaptic current (IPSC) recorded at different holding potentials from −80 to −40 mV in whole-cell patch-clamp configuration in CA1 hippocampal neurons from WT (black) and R6/2 (green) or YAC128 (orange) mice. *Insets* show sample traces of the corresponding current induced by electrical stimulation in the presence of the glutamate blocker DNQX (20 μM). (Scale bars: 40 pA and 10 ms for *A*; 100 pA and 10 ms for *F*.) E_{GABA} is shown at the arrow. (*B*) Summary of individual E_{GABA} recordings obtained from all IV curves in WT ($n = 8$) and R6/2 ($n = 11$) ($P = 0.0009$; Student's unpaired *t* test). (*C*) Similar to *B*, but for E_{GABA} using Cl^- loading whole-cell patch-clamp recording between WT ($n = 9$) and R6/2 ($n = 13$) ($P = 0.010$; Student's unpaired *t* test); gramicidin perforated recording between WT ($n = 6$) and R6/2 ($n = 7$) ($P = 0.029$; Student's unpaired *t* test). (*D*) Similar to *B* but for resting membrane potential (RMP) from WT ($n = 8$) and R6/2 ($n = 11$) ($P = 0.412$; Student's unpaired *t* test). (*E*) Similar to *B* but for synaptic conductance from WT ($n = 8$) and R6/2 ($n = 11$) ($P = 0.977$; Student's unpaired *t* test). (*G*) Similar to *B* but for E_{GABA} from WT ($n = 7$) and YAC128 ($n = 13$) ($P = 0.004$; Student's unpaired *t* test). (*H*) Similar to *B* but for RMP in WT ($n = 7$) and YAC128 ($n = 13$) ($P = 0.973$; Student's unpaired *t* test). For all panels, circles indicate values from single recordings across a minimum of three mice, and all summary figures represent mean ± SEM. $^*P < 0.05$, $^{**}P < 0.01$, $^{***}P < 0.001$.

R6/2 mice. Our results showed that the baseline spiking activity was significantly higher in R6/2 (0.25 ± 0.04 Hz) compared with WT mice (0.07 ± 0.01 Hz) ($P = 0.001$), which was abolished by application of the $GABA_A$ receptor antagonist bicuculline (Fig. 4 *A* and *B*).

The depolarization of E_{GABA} also suggests that GABAergic transmission may be excitatory. To determine if GABA is excitatory in the hippocampus of R6/2 mice, we tested the effect of GABA application on spike frequency. Specifically, we made cell-attached patch-clamp recordings from CA1 pyramidal neurons during bath application of increasing concentrations of exogenous GABA. GABA application at increasing concentrations in WT neurons did not result in spiking, consistent with the known inhibitory action of GABA in the adult brain. However, GABA application at the same concentrations elicited a strong increase in spike frequency in neurons from R6/2 mice (Fig. 4 *C* and *D*), which was abolished by application of the $GABA_A$ receptor antagonist bicuculline (*SI Appendix*, Fig. S8).

NKCC1 Is Responsible for Depolarized E_{GABA} in R6/2 Hippocampal Neurons. We next asked whether the depolarizing shift of the GABA reversal potential is due primarily to an increase in NKCC1 and/or a decrease in KCC2 expression. To answer this question, we first determined the effect of the FDA-approved NKCC1 inhibitor bumetanide on E_{GABA}. In WT CA1 pyramidal neurons, bumetanide did not significantly change E_{GABA} (Fig. 5 *A*–*C*; E_{GABA} change: −1.34 ± 1.40 mV; $P = 0.37$), consistent with the known low expression of NKCC1 in mature neurons (45, 46). In contrast, bumetanide produced a significant hyperpolarization of E_{GABA} in neurons from R6/2 mice (Fig. 5 *A*–*C*; E_{GABA} change: −6.22 ± 0.76 mV; $P = 0.01$), consistent with the increased expression of NKCC1 we observed in Fig. 1*C*. To isolate the contribution of KCC2 to E_{GABA}, we performed an occlusion experiment using furosemide (1 mM), which is an NKCC1 and KCC2 inhibitor, together with the NKCC1 inhibitor bumetanide. As expected, E_{GABA} in WT neurons depolarized after KCC2 inhibition with furosemide (in the presence of bumetanide) (Fig. 5 *A*–*C*; E_{GABA} change: 10.46 ± 1.70 mV; $P = 0.0009$), while E_{GABA} did not significantly change in R6/2 neurons (Fig. 5 *A*–*C*; E_{GABA} change: 1.10 ± 1.05 mV; $P = 0.33$). This suggests that relatively high expression of NKCC1 accounts for the relatively depolarized E_{GABA} in hippocampal pyramidal neurons of R6/2 mice. We also asked whether inhibitory synapses in R6/2 following treatment with bumetanide are functionally similar to WT animals [in artificial cerebrospinal fluid (aCSF)]. We answered this question by comparing inhibitory synaptic conductance between the two groups and found no significant difference in conductance between WT (aCSF) and R6/2 treated with bumetanide ($P = 0.70$) (Fig. 5*D*), suggesting that inhibitory synapses are not significantly altered presymptomatically in the R6/2 hippocampus.

Having determined that bumetanide can hyperpolarize E_{GABA} in CA1 pyramidal neurons from R6/2 mice, we next asked whether bumetanide can abolish the excitatory action of GABA

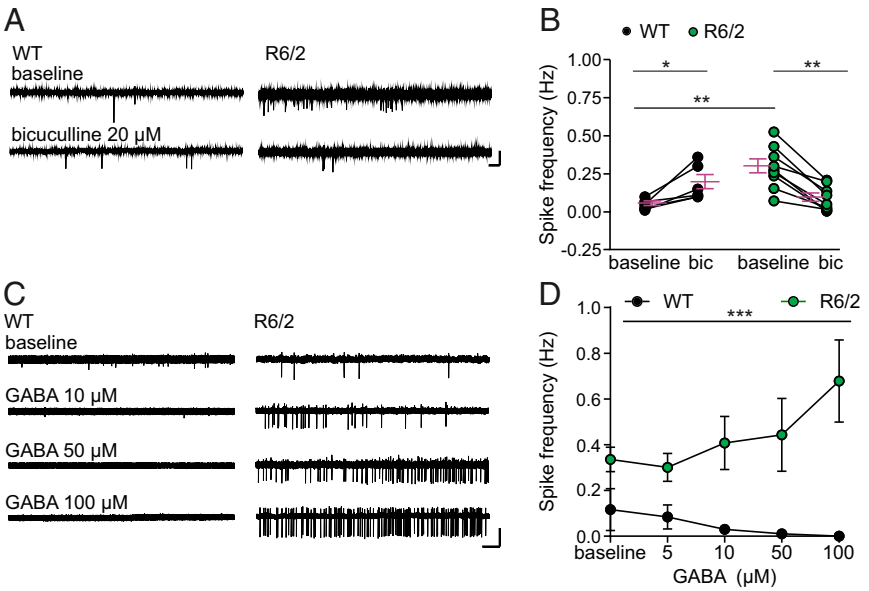

Fig. 4. R6/2 mice exhibit excitatory responses to the exogenous application of GABA. (*A*) Sample traces of spontaneous spiking activity in cell-attached patch-clamp configuration in acute slices derived from R6/2 mice and WT littermates at baseline and after bath application of bicuculline (20 μM). (Scale bars: 50 pA and 10 s.) (*B*) Quantification of the mean ± SEM before and after application of bicuculline (20 μM) in neurons from R6/2 ($n = 9$; $P = 0.003$; Wilcoxon matched-pairs signed-rank test) and WT ($n = 6$; $P = 0.049$; Student's paired t test). The difference between spiking activity in WT and R6/2 mice was determined using Mann–Whitney test ($P = 0.001$). (*C*) Example traces of spontaneous spiking in R6/2 mice and WT littermates before (baseline) and during bath application of GABA at different concentrations (10, 50, and 100 μM). (Scale bars: 50 pA and 5 s.) (*D*) Quantification of the mean ± SEM summarizing the effect of GABA application on spontaneous spiking activity in neurons from R6/2 mice ($n = 14$ for the baseline, $n = 12$ for GABA 5 μM, $n = 11$ for 10 μM, and $n = 10$ for 50 and 100 μM) and WT mice ($n = 8$ for the baseline and $n = 6$ for 5, 10, 50, and 100 GABA application). Significant differences were determined by comparison with baseline frequencies using two-way repeated-measure analysis of variance (ANOVA) ($F_{1,\ 79} = 28.66$; $P < 0.0001$) followed by Sidak's multiple comparisons test ($P < 0.01$). (*C*) Sample traces of spontaneous spiking activity in neurons from WT and R6/2 mice before and after bath application of bicuculline (20 μM). (Scale bars: 50 pA and 10 s.) *$P < 0.05$, **$P < 0.01$, ***$P < 0.001$.

(Fig. 4). We repeated our experiments determining the effect of GABA on spike frequency and found that bumetanide abolished GABA-induced spiking ($P = 0.02$; Fig. 5 *E* and *F*), while not altering spontaneous spiking activity in WT neurons ($P = 0.65$; Fig. 5 *E* and *F*).

Bumetanide Treatment Rescues Memory Deficits in R/2 Mice. Human HD patients display deficits in spatial and recognition learning and memory tasks (3, 4), and these behavioral deficits have been replicated in HD mouse models including R6/2 (5, 6, 10). We hypothesized that the GABA-mediated excitation contributes to the learning and memory deficits in R6/2 mice in the early stages of the disease before prominent motor deficits are observed. To test this hypothesis, we evaluated hippocampal-dependent learning and memory tasks after 1 and 2 wk of systemic bumetanide i.p. injection (0.2 mg·kg^{-1} i.p. daily; Fig. 6*A*). We subjected the mice to the T-maze spontaneous alternation task, the novel object recognition test (NORT), and novel object location test (NOLT), which enable testing of spatial memory performance and long-term memory. Consistent with a previous study (10), we observed that R6/2 mice with saline injection made significantly fewer alternations in the T-maze, indicating poor spatial memory performance (Fig. 6*B*). Neither group differed in their mean latency to enter the arms, which indicates that R6/2 mice did not have impairments in locomotor activity (*SI Appendix*, Fig. S9). R6/2 mice also showed poor novelty-discrimination capability in the NORT compared with WT littermates (Fig. 6*C*), with no object preference in the NOLT (Fig. 6*D*). Bumetanide administration by daily i.p. injection for either 1 or 2 wk restored the poor T-maze alternation performance of R6/2 mice (Fig. 6*B*), indicating a recovery of spatial-memory performance. Consistently, R6/2 mice with bumetanide administration performed as well as WT mice in NOLT (Fig. 6*D*). In NORT, we found that the poor novelty-discrimination capability of R6/2 mice after 24 h was rescued by bumetanide administration (Fig. 6*C*).

To determine whether the effect of bumetanide is long-lasting, we performed electrophysiological experiments on mice at the end of behavioral testing, after bumetanide had been washed out. We discovered that in the absence of continual bumetanide, E_{GABA} in previously administrated R6/2 mice with bumetanide was depolarized to the point where it was in R6/2 mice with saline injection and not significantly different ($P = 0.88$) (*SI Appendix*, Fig. S10).

Previous studies have reported that brain penetration of bumetanide may not be optimal following systemic administration, due to its pharmacokinetic properties (47, 48). To address this, we used micro-osmotic pumps implanted into the lateral ventricle of the brain (Fig. 6*A*; 0.8 mg·kg·h) and repeated the behavioral tests. Consistent with i.p. injection, we found that the spatial memory deficits in R6/2 mice were rescued following 1 or 2 wk of administration of bumetanide (Fig. 6*E*). We also retested the R6/2 mice on NORT and NOLT and found that the brain infusion of bumetanide rescues the memory deficits in R6/2 mice (Fig. 6 *F* and *G*).

Discussion

In the present study, we discovered that aberrant hippocampal GABAergic signaling through $GABA_A$ receptors contributes to the learning and memory deficits in the R6/2 mouse model of HD. Specifically, we found that cation-chloride cotransporter expression is altered in the hippocampus and results in depolarized E_{GABA} in both the R6/2 and YAC128 HD mouse models, which renders GABA an excitatory neurotransmitter. Inhibition of the Cl^--importing transporter NKCC1 with the FDA-approved bumetanide restored hyperpolarizing GABAergic inhibition and rescued hippocampal-dependent learning and memory deficits.

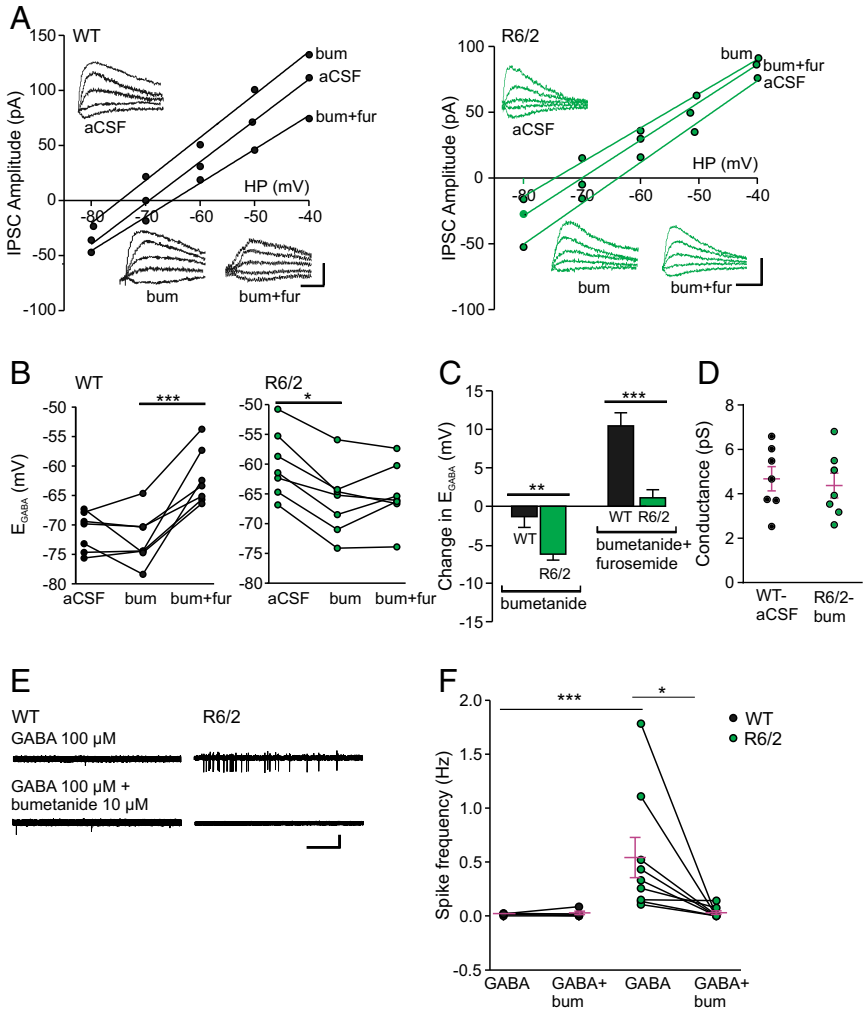

Fig. 5. Inhibition of NKCC1 with bumetanide hyperpolarizes E_{GABA} and reverses the excitatory action of GABA in R6/2 hippocampal neurons. (*A*) Example current–voltage curves of inhibitory postsynaptic current (IPSC) recorded in whole-cell patch-clamp recording configuration showing E_{GABA} at different holding potentials from WT mice before, 20 min after perfusion with the NKCC1 inhibitor bumetanide (10 µM), and 20 min after application of bumetanide and the KCC2 and NKCC1 blocker, furosemide (1 mM). *Insets* show the sample traces of the corresponding current for WT and R6/2. (Scale bars: 100 pA, and 10 ms.) (*B*) Summary of E_{GABA} before and after application of bumetanide and furosemide in WT ($n = 7$; bum, $P = 0.373$; bum + fur, $P = 0.0009$; Student's paired *t* test) and R6/2 ($n = 7$; bum, $P = 0.015$; bum + fur, $P = 0.468$; Wilcoxon matched-pairs signed rank test). Bum, bumetanide; fur, furosemide. (*C*) Summary graph showing the changes in E_{GABA} in the presence of bumetanide alone ($P = 0.009$; Student's unpaired *t* test) and bumetanide and furosemide together ($P = 0.0005$; Student's unpaired *t* test). (*D*) Summary of individual synaptic conductance obtained from the slope of the IV curves in WT-aCSF ($n = 7$) and R6/2 treated with bumetanide ($n = 7$) ($P = 0.7038$; Student's unpaired *t* test). (*E*) Sample traces of spontaneous spiking activity in WT (*Left*) and R6/2 (*Right*) from CA1 neurons in the presence of GABA 100 µM with and without bumetanide (10 µM). (Scale bars: 50 pA and 20 s.) (*F*) Quantification of spike frequency before and after application of bumetanide in WT ($n = 5$; $P = 0.625$; Student's paired *t* test) and R6/2 ($n = 9$; $P = 0.0294$; Student's paired *t* test). The difference between spiking activity between WT and R6/2 mice was determined using Mann–Whitney test ($P = 0.001$). $^*P < 0.05$, $^{**}P < 0.01$, $^{***}P < 0.001$.

Taken together, these findings suggest bumetanide as a potential therapy for the treatment of early cognitive deficits in human HD patients.

Recent proteomic and bioinformatic data linked (m)Htt and KCC2 (25, 26), and in the present study, we provide the biochemical validation of this protein interaction. We found that KCC2 interacts with both Htt and mHtt and KCC2 protein expression is decreased in the hippocampus of two predominant mouse models of HD (R6/2 and YAC128), consistent with a recent report of decreased KCC2 protein expression in the cortex and striatum of R6/2 mice (49). While a decrease in *Slc12A5* mRNA accounts for some of the reduction in KCC2 protein expression, there is still KCC2 protein present in hippocampal neurons of HD mouse models, and thus additional mechanisms likely also regulate KCC2 protein expression. The expanded polyglutamine repeat in mHtt is toxic and can cause aberrant protein–protein interactions, which interfere with the function and expression of diverse cellular proteins (50). mHtt aggregates intracellularly, and thus KCC2 may be sequestered into the protein aggregates. However, it is also possible that the mHtt effect on KCC2 is indirect and mediated by additional protein interactions. For example, Htt interacts with brain-type creatine kinase (CKB), an enzyme involved in energy homeostasis (26, 49, 51). Reduced expression of CKB in neurons expressing mHtt is a key event in the pathogenesis of HD and contributes to the neuronal dysfunction associated with HD (51). CKB also interacts, phosphorylates, and activates KCC2 transporter function (52). Therefore, the decreased KCC2 expression in the R6/2 hippocampus may result from the reduced CKB-mediated phosphorylation and activation of KCC2.

In addition to a decrease in KCC2 expression, we also found a significant increase in NKCC1 protein in R6/2 mice, despite

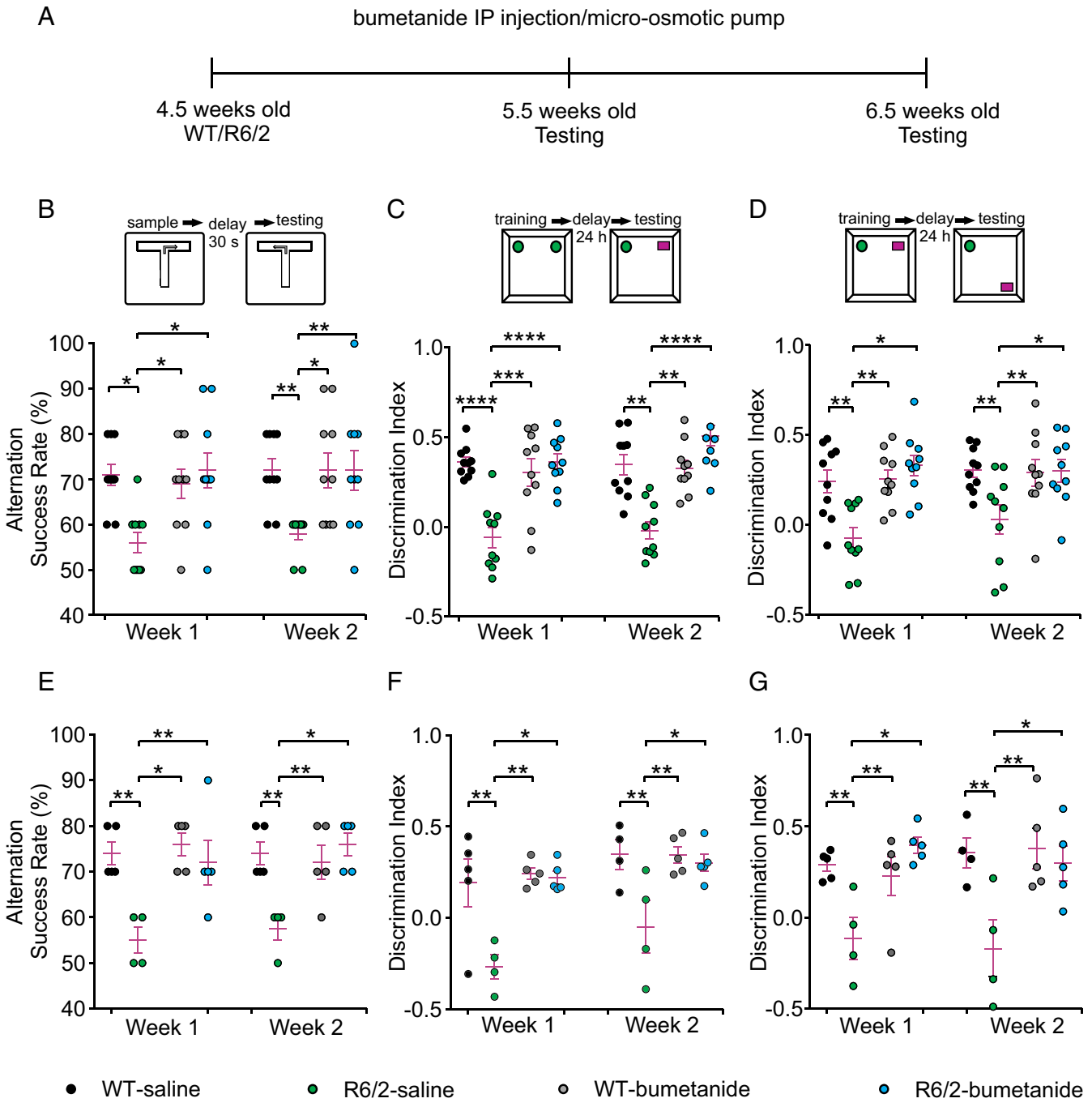

Fig. 6. Treatment with bumetanide restores memory function in behavioral tasks in R6/2 mice. (*A*) A schematic representation of the experimental protocol. (*B*, *Top*) A schematic representation of T-maze spontaneous alternation test. (*B*, *Bottom*) Quantification of alternation success rate in mice treated with vehicle or bumetanide using i.p. injection ($n = 10$ for all groups). (*C*, *Top*) A schematic representation of NORT. Quantification of NORT results in mice treated with vehicle or bumetanide using i.p. injection ($n = 10$ for all groups). (*D*, *Top*) A schematic representation of NOLT. Quantification of NOLT results in mice treated with vehicle or bumetanide using i.p. injection ($n = 10$ for all groups). (*E*) Quantification of alternation success in mice treated with vehicle or bumetanide using micro-osmotic pumps ($n = 4$–5 for all groups). (*F*) Quantification of NORT results in mice treated with vehicle or bumetanide using micro-osmotic pumps ($n = 4$ or 5 for all groups). (*G*) Quantification of NOLT results in mice treated with vehicle or bumetanide using micro-osmotic pumps ($n = 4$ or 5 for all groups). Two-way ANOVA used followed by Tukey's multiple comparison test ($P < 0.05$) was used for all of the graphs. All statistical details are in *SI Appendix*, Tables S2 and S3. Circles indicate values from single animals, and all summary figures represent mean ± SEM. *$P < 0.05$, **$P < 0.01$, ***$P < 0.001$, ****$P < 0.0001$.

the fact that NKCC1 does not interact with Htt. Increases in NKCC1 have been previously reported when disruptions in KCC2 are observed and are thought to represent a reversion to an immature GABAergic phenotype (38, 53). However, it is also possible that the increase in NKCC1 results from the secondary effects of toxic mHtt. For example, mHtt impairs brain-derived neurotrophic factor (BDNF) gene transcription and reduces the expression of the BDNF in HD patients and mouse models of HD (54). BDNF has been reported to regulate NKCC1 protein expression. NKCC1 was increased in the rat hippocampus of pilocarpine-induced temporal lobe epilepsy, which was decreased by BDNF application (55). Dysregulation of BDNF in

HD could be a reason for altered NKCC1 protein we observed in this study. While we did not observe an increase in NKCC1 protein in YAC128 mice, this may be due to the delay in onset of behavioral symptoms in full-length transgenic HD models (56). The mechanism underlying the increase in NKCC1 protein expression in the R6/2 hippocampus is not clear. While our real-time qPCR results do not indicate an increase in *Slc12A2*, subtle gene expression difference is challenging to detect. This is especially true in HD, where transcriptional dysregulation is a central pathogenic mechanism underlying the disease.

Presymptomatic HD patients show deficits in attention, working memory, verbal learning, verbal long-term memory, and learning of random associations, and these deficits are the earliest cognitive manifestations in HD-gene carriers (3). These tasks, at least in part, are regulated by the hippocampus (57–60). Hippocampal-dependent behaviors depend on changes in synaptic function and plasticity (61), and mouse models of HD have alterations in hippocampal excitatory synaptic plasticity (5, 7–10, 62–64). Electrophysiological assessment of hippocampal function has shown that basal neurotransmission at hippocampal synapses (CA3–CA1 field excitatory postsynaptic potentials) appears normal, whereas long-term potentiation (LTP) is reduced in transgenic (5) and knock-in (6, 7) mouse models of HD. Our study provides direct evidence that reduced inhibition contributes to the learning and memory deficits in the early stages of HD. KCC2-mediated Cl^- regulation directly controls synapse specificity of LTP at CA1 synapses in mature animals (23); thus, it is possible that the reduction in inhibition we observe in the hippocampus of R6/2 mice leads to a reduction of synapse-specific LTP, which in turn is responsible for the reduced performance of R6/2 mice on hippocampal-dependent learning and memory tests.

The alterations in cation-chloride cotransporters in R6/2 hippocampal neurons resulted in a depolarization of E_{GABA} that was significant enough to render GABA excitatory. By performing a pharmacological occlusion experiment, we determined that excitatory GABA primarily resulted from the NKCC1-mediated transport of Cl^- into the neuron. Consistently, bumetanide treatment decreased spontaneous and exogenous GABA-induced spiking in R6/2 neurons and rescued hippocampal-associated learning and memory test performance. This is line with previous literature showing that bumetanide reverses excitatory GABA and improves behavioral outcomes in animal models of Down syndrome (21), ASD (22), epilepsy (38), and seizure (65).

Bumetanide has been used previously to improve behavioral phenotypes in patients with various neurological disorders where intracellular Cl^- is high and inhibition is disrupted, including ASD (66), schizophrenia (67), and Parkinson's disease (68). Although bumetanide effectiveness in humans may be further improved with regard to target specificity and blood–brain barrier penetration (47), our behavioral results suggest that a systemic i.p. injection is sufficient to improve learning and memory deficits seen in R6/2 mice. HD is classically considered a motor disorder, however the cognitive and behavioral impairments emerge in the early stages of the disease and precede the motor impairments by ∼15 y, producing a significant burden on caregivers (4). Our findings describe a safe pharmacological approach to reduce cognitive dysfunction in HD that can improve patient quality of life and reduce caregiver burden.

Materials and Methods

More detailed information on materials and methods is provided in *SI Appendix, SI Materials and Methods*.

Animals. All animal procedures were approved by the University of Toronto Animal Care Committee in accordance with the Canadian Council for Animal Care guidelines. All efforts were made to minimize animal suffering and to reduce the number of animals used. Two HD mouse models were used in this study: transgenic R6/2 mice containing the mutated Htt gene expressing exon 1 of the human Htt gene carrying ∼120 ± 5 CAG repeat expansions (31) and YAC128 mice containing full-length human Htt with 128 CAG repeats (37). Both males and females were used for biochemistry, imaging, electrophysiology, and behavioral experiments.

Biochemistry and Imaging. Antibodies used in this study have been described previously, as have the methods for immunoblotting, imaging, and immunoprecipitation (69).

Electrophysiology. To estimate GABA reversal potential (E_{GABA}), we performed whole-cell and perforated patch-clamp recordings. To record GABA spiking activity, we used cell-attached voltage-clamp configuration and perfused the slices with aCSF and GABA at increasing concentration (21).

Behavioral Testing. For behavioral experiments, R6/2 and WT littermates were randomly assigned to bumetanide (0.2 mg/kg body weight or 2% DMSO in saline; Sigma) for daily i.p. injection or (6 mg/mL bumetanide in 50% DMSO/15% EtOH or 50% DMSO/15% EtOH in ddH2O) for micro-osmotic infusion pumps. On the day of behavioral testing, i.p. injections were given at least 1 h before the beginning of the task. For micro-osmotic pump implantations, we targeted the lateral ventricle to deliver bumetanide via ALZET brain infusion kit cannula (#0008851; ALZET). The pumps were then surgically implanted s.c. on the animal's back.

ACKNOWLEDGMENTS. We thank Michael Hayden (University of British Columbia) for Htt constructs and Thanh Nguyen for technical assistance. This work was supported by the following funding sources: a Canadian Institutes of Health Research (CIHR) grant (to M.A.W.); Natural Sciences and Engineering Research Council of Canada (NSERC) Discovery Grant MOP 491009 and CIHR Grant MOP 496401 (to J.C.K.); an Ontario Graduate Scholarship (OGS) (Z.D.); and a Brazilian National Council for Scientific and Technological Development (CNPq, Conselho Nacional de Desenvolvimento Científico e Tecnológico) postdoctoral fellowship (G.M.P.).

1. Zuccato C, Valenza M, Cattaneo E (2010) Molecular mechanisms and potential therapeutical targets in Huntington's disease. *Physiol Rev* 90:905–981.
2. Begeti F, Schwab LC, Mason SL, Barker RA (2016) Hippocampal dysfunction defines disease onset in Huntington's disease. *J Neurol Neurosurg Psychiatry* 87:975–981.
3. Lemiere J, Decruyenaere M, Evers-Kiebooms G, Vandenbussche E, Dom R (2004) Cognitive changes in patients with Huntington's disease (HD) and asymptomatic carriers of the HD mutation–A longitudinal follow-up study. *J Neurol* 251:935–942.
4. Paulsen JS (2011) Cognitive impairment in Huntington disease: Diagnosis and treatment. *Curr Neurol Neurosci Rep* 11:474–483.
5. Murphy KP, et al. (2000) Abnormal synaptic plasticity and impaired spatial cognition in mice transgenic for exon 1 of the human Huntington's disease mutation. *J Neurosci* 20:5115–5123.
6. Usdin MT, Shelbourne PF, Myers RM, Madison DV (1999) Impaired synaptic plasticity in mice carrying the Huntington's disease mutation. *Hum Mol Genet* 8:839–846.
7. Lynch G, et al. (2007) Brain-derived neurotrophic factor restores synaptic plasticity in a knock-in mouse model of Huntington's disease. *J Neurosci* 27:4424–4434.
8. Simmons DA, et al. (2009) Up-regulating BDNF with an ampakine rescues synaptic plasticity and memory in Huntington's disease knockin mice. *Proc Natl Acad Sci USA* 106:4906–4911.
9. Kolodziejczyk K, Parsons MP, Southwell AL, Hayden MR, Raymond LA (2014) Striatal synaptic dysfunction and hippocampal plasticity deficits in the Hu97/18 mouse model of Huntington disease. *PLoS One* 9:e94562.
10. Lione LA, et al. (1999) Selective discrimination learning impairments in mice expressing the human Huntington's disease mutation. *J Neurosci* 19:10428–10437.
11. Donato F, Rompani SB, Caroni P (2013) Parvalbumin-expressing basket-cell network plasticity induced by experience regulates adult learning. *Nature* 504:272–276.
12. Lovett-Barron MM, et al. (2014) Dendritic inhibition in the hippocampus supports fear learning. *Science* 343:857–863.
13. Murray AJ, et al. (2011) Parvalbumin-positive CA1 interneurons are required for spatial working but not for reference memory. *Nat Neurosci* 14:297–299.
14. Palop JJ, et al. (2007) Aberrant excitatory neuronal activity and compensatory remodeling of inhibitory hippocampal circuits in mouse models of Alzheimer's disease. *Neuron* 55:697–711.
15. Verret L, et al. (2012) Inhibitory interneuron deficit links altered network activity and cognitive dysfunction in Alzheimer model. *Cell* 149:708–721.
16. Schmid LCC, et al. (2016) Dysfunction of somatostatin-positive interneurons associated with memory deficits in an Alzheimer's disease model. *Neuron* 92:114–125.
17. Farrant M, Kaila K (2007) The cellular, molecular and ionic basis of GABA(A) receptor signalling. *Prog Brain Res* 160:59–87.
18. Rivera C, et al. (1999) The K+/Cl- co-transporter KCC2 renders GABA hyperpolarizing during neuronal maturation. *Nature* 397:251–255.
19. Kaila K, Price TJ, Payne JA, Puskarjov M, Voipio J (2014) Cation-chloride cotransporters in neuronal development, plasticity and disease. *Nat Rev Neurosci* 15:637–654.

20. Kahle KT, et al. (2014) Genetically encoded impairment of neuronal KCC2 cotransporter function in human idiopathic generalized epilepsy. *EMBO Rep* 15:766–774.
21. Deidda G, et al. (2015) Reversing excitatory GABAAR signaling restores synaptic plasticity and memory in a mouse model of Down syndrome. *Nat Med* 21:318–326.
22. Tyzio R, et al. (2014) Oxytocin-mediated GABA inhibition during delivery attenuates autism pathogenesis in rodent offspring. *Science* 343:675–679.
23. Ferando I, Faas GC, Mody I (2016) Diminished KCC2 confounds synapse specificity of LTP during senescence. *Nat Neurosci* 19:1197–1200.
24. Li SH, Li XJ (2004) Huntingtin-protein interactions and the pathogenesis of Huntington's disease. *Trends Genet* 20:146–154.
25. Culver BP, et al. (2012) Proteomic analysis of wild-type and mutant huntingtin-associated proteins in mouse brains identifies unique interactions and involvement in protein synthesis. *J Biol Chem* 287:21599–21614.
26. Shirasaki DI, et al. (2012) Network organization of the huntingtin proteomic interactome in mammalian brain. *Neuron* 75:41–57.
27. Kalathur RKR, et al. (2015) The unfolded protein response and its potential role in Huntington's disease elucidated by a systems biology approach. *F1000 Res* 4:103.
28. Matus S, Glimcher LH, Hetz C (2011) Protein folding stress in neurodegenerative diseases: A glimpse into the ER. *Curr Opin Cell Biol* 23:239–252.
29. Vidal R, Caballero B, Couve A, Hetz C (2011) Converging pathways in the occurrence of endoplasmic reticulum (ER) stress in Huntington's disease. *Curr Mol Med* 11:1–12.
30. Forman MS, Lee VMY, Trojanowski JQ (2003) 'Unfolding' pathways in neurodegenerative disease. *Trends Neurosci* 26:407–410.
31. Mangiarini L, et al. (1996) Exon 1 of the HD gene with an expanded CAG repeat is sufficient to cause a progressive neurological phenotype in transgenic mice. *Cell* 87: 493–506.
32. Blaesse P, et al. (2006) Oligomerization of KCC2 correlates with development of inhibitory neurotransmission. *J Neurosci* 26:10407–10419.
33. Uvarov P, et al. (2009) Coexpression and heteromerization of two neuronal K-Cl cotransporter isoforms in neonatal brain. *J Biol Chem* 284:13696–13704.
34. Modregger J, DiProspero NA, Charles V, Tagle DA, Plomann M (2002) PACSIN 1 interacts with huntingtin and is absent from synaptic varicosities in presymptomatic Huntington's disease brains. *Hum Mol Genet* 11:2547–2558.
35. Pérez-Otaño I, et al. (2006) Endocytosis and synaptic removal of NR3A-containing NMDA receptors by PACSIN1/syndapin1. *Nat Neurosci* 9:611–621.
36. Goehler H, et al. (2004) A protein interaction network links GIT1, an enhancer of huntingtin aggregation, to Huntington's disease. *Mol Cell* 15:853–865, and erratum (2005) 19:287.
37. Slow EJ, et al. (2003) Selective striatal neuronal loss in a YAC128 mouse model of Huntington disease. *Hum Mol Genet* 12:1555–1567.
38. Palma E, et al. (2006) Anomalous levels of Cl- transporters in the hippocampal subiculum from temporal lobe epilepsy patients make GABA excitatory. *Proc Natl Acad Sci USA* 103:8465–8468.
39. Kahle KT, et al. (2008) Roles of the cation-chloride cotransporters in neurological disease. *Nat Clin Pract Neurol* 4:490–503.
40. Ben-Ari Y (2002) Excitatory actions of gaba during development: The nature of the nurture. *Nat Rev Neurosci* 3:728–739.
41. Benn CL, Fox H, Bates GP (2008) Optimisation of region-specific reference gene selection and relative gene expression analysis methods for pre-clinical trials of Huntington's disease. *Mol Neurodegener* 3:17.
42. Dzhala VI, et al. (2005) NKCC1 transporter facilitates seizures in the developing brain. *Nat Med* 11:1205–1213.
43. Hewitt SA, Wamsteeker JI, Kurz EU, Bains JS (2009) Altered chloride homeostasis removes synaptic inhibitory constraint of the stress axis. *Nat Neurosci* 12:438–443.
44. Doyon N, Vinay L, Prescott SA, De Koninck Y (2016) Chloride regulation: A dynamic equilibrium crucial for synaptic inhibition. *Neuron* 89:1157–1172.
45. Payne JA, Rivera C, Voipio J, Kaila K (2003) Cation-chloride co-transporters in neuronal communication, development and trauma. *Trends Neurosci* 26:199–206.
46. Blaesse P, Airaksinen MS, Rivera C, Kaila K (2009) Cation-chloride cotransporters and neuronal function. *Neuron* 61:820–838.
47. Puskarjov M, Kahle KT, Ruusuvuori E, Kaila K (2014) Pharmacotherapeutic targeting of cation-chloride cotransporters in neonatal seizures. *Epilepsia* 55:806–818.
48. Löscher W, Puskarjov M, Kaila K (2013) Cation-chloride cotransporters NKCC1 and KCC2 as potential targets for novel antiepileptic and antiepileptogenic treatments. *Neuropharmacology* 69:62–74.
49. Hsu Y-T, et al. (2017) Altered behavioral responses to gamma-aminobutyric acid pharmacological agents in a mouse model of Huntington's disease. *Mov Disord* 32: 1600–1609.
50. Cattaneo E, et al. (2001) Loss of normal huntingtin function: New developments in Huntington's disease research. *Trends Neurosci* 24:182–188.
51. Lin YS, Cheng TH, Chang CP, Chen HM, Chern Y (2013) Enhancement of brain-type creatine kinase activity ameliorates neuronal deficits in Huntington's disease. *Biochim Biophys Acta* 1832:742–753.
52. Inoue K, Yamada J, Ueno S, Fukuda A (2006) Brain-type creatine kinase activates neuron-specific K+-Cl- co-transporter KCC2. *J Neurochem* 96:598–608.
53. Huberfeld G, et al. (2007) Perturbed chloride homeostasis and GABAergic signaling in human temporal lobe epilepsy. *J Neurosci* 27:9866–9873.
54. Giralt A, et al. (2009) Brain-derived neurotrophic factor modulates the severity of cognitive alterations induced by mutant huntingtin: Involvement of phospholipaseCgamma activity and glutamate receptor expression. *Neuroscience* 158:1234–1250.
55. Eftekhari S, et al. (2014) BDNF modifies hippocampal KCC2 and NKCC1 expression in a temporal lobe epilepsy model. *Acta Neurobiol Exp (Warsz)* 74:276–287.
56. Pouladi MA, Morton AJ, Hayden MR (2013) Choosing an animal model for the study of Huntington's disease. *Nat Rev Neurosci* 14:708–721.
57. Kessels RPC, de Haan EHF, Kappelle LJ, Postma A (2001) Varieties of human spatial memory: A meta-analysis on the effects of hippocampal lesions. *Brain Res Brain Res Rev* 35:295–303.
58. Clarke JR, Cammarota M, Gruart A, Izquierdo I, Delgado-García JM (2010) Plastic modifications induced by object recognition memory processing. *Proc Natl Acad Sci USA* 107:2652–2657.
59. Burgess N, Maguire EA, O'Keefe J (2002) The human hippocampus and spatial and episodic memory. *Neuron* 35:625–641.
60. Montaldi D, Mayes AR (2010) The role of recollection and familiarity in the functional differentiation of the medial temporal lobes. *Hippocampus* 20:1291–1314.
61. Bliss TV, Collingridge GL (1993) A synaptic model of memory: Long-term potentiation in the hippocampus. *Nature* 361:31–39.
62. Giralt A, et al. (2011) Increased PKA signaling disrupts recognition memory and spatial memory: Role in Huntington's disease. *Hum Mol Genet* 20:4232–4247.
63. Brito V, et al. (2014) Neurotrophin receptor p75(NTR) mediates Huntington's disease-associated synaptic and memory dysfunction. *J Clin Invest* 124:4411–4428.
64. Hodgson JG, et al. (1999) A YAC mouse model for Huntington's disease with full-length mutant huntingtin, cytoplasmic toxicity, and selective striatal neurodegeneration. *Neuron* 23:181–192.
65. Dzhala VI, et al. (2010) Progressive NKCC1-dependent neuronal chloride accumulation during neonatal seizures. *J Neurosci* 30:11745–11761.
66. Lemonnier E, et al. (2013) Treating Fragile X syndrome with the diuretic bumetanide: A case report. *Acta Paediatr* 102:e288–e290.
67. Lemonnier E, Lazartigues A, Ben-Ari Y (2016) Treating schizophrenia with the diuretic bumetanide: A case report. *Clin Neuropharmacol* 39:115–117.
68. Damier P, Hammond C, Ben-Ari Y (2016) Bumetanide to treat Parkinson disease: A report of 4 cases. *Clin Neuropharmacol* 39:57–59.
69. Mahadevan V, et al. (2014) Kainate receptors coexist in a functional complex with KCC2 and regulate chloride homeostasis in hippocampal neurons. *Cell Rep* 7:1762–1770.